Ion Current Calculations Based on Three Dimensional Poisson−Nernst−Planck Theory for a Cyclic Peptide Nanotube

Hyonseok Hwang, George C. Schatz,* and Mark A. Ratner

Department of Chemistry, Northwestern University, 2145 Sheridan Road, Evanston, Illinois 60208-3113

Received: October 8, 2005; In Final Form: January 12, 2006

Ion current calculations based on Poisson−Nernst−Planck (PNP) theory are performed for a synthetic cyclic peptide nanotube that consists of eight or ten cyclo[(-L-Trp-D-Leu-)$_4$] embedded in a lipid bilayer membrane to investigate the ion transport properties of the nanotube. To explore systems with arbitrary geometries, three-dimensional PNP theory is implemented using a finite difference method. The influence of dipolar lipid molecules on the ion currents is also examined by turning on or off the charges of the lipid dipoles in dipalmitoylphosphatidylcholine (DPPC). Comparisons between the calculated and experimentally measured ion currents show that the PNP approach agrees well with the measurements at low ion concentrations but overestimates the currents at higher concentrations. Concentration profiles reveal the selectivity of the peptide nanotube to cations, which is attributed to the negatively charged carbonyl oxygens inside the nanotube. The dominant cation and the minimum anion concentrations inside the cyclic peptide nanotube suggest that these cyclic peptide nanotubes can be employed as ion sensors. In the case of the polar DPPC bilayer, smaller currents are obtained in the calculation. The variation of current with polarity of the lipids implies that both polar and nonpolar lipid bilayer membranes can be utilized to regulate ion currents in the peptide nanotube and other ion channels. Strengths and limitations of the PNP theory are also discussed.

I. Introduction

Ion channels are a class of proteins that are composed of macromolecular pores and which regulate ion transport across lipid bilayer membranes. Ion channels play a crucial role in fundamental biological processes such as neurotransmission.[1−3] They can also operate as biosensors to detect ions or small biomolecules due to their selectivity and sensitivity.[4] Because of their significance and medical applications, studies of ion channels have long been an important field in basic and applied sciences.

Synthetic ion channels possess similar properties to natural ion channels and have been considered as nanoscale biosensor devices due to their relatively simple structures.[5−7] Among the synthetic ion channels are several types of cyclic peptide nanotubes synthesized by Ghadiri et al. based on the self-assembly of rationally designed cyclic peptides that have a closed ring with an even number of alternating D- and L-amino acid residues.[8−13] These rings can self-assemble into tubular structures as a result of hydrogen bonding, and it is these tubes that are used as ion channels. Depending on the hydrophobic or hydrophilic nature of the side chains, the self-assembled nanotube can be found either in lipid bilayer membranes or in water solution.[8,9,12] In single channel experiments with these tubes, Ghadiri et al. showed that they exhibit conductance and rectification properties and suggested that the peptide nanotubes can be utilized in the design of stochastic sensing devices.[13]

Changes in the electrostatic potential at a membrane/water interface due to dipoles in the lipid have substantial influence on the conductance of ions through an ion channel. Numerous experimental and theoretical studies have been devoted to measuring and calculating these interfacial electrostatic potentials.[13−19] Among these studies, Gawrisch et al. used two different lipid molecules, dipalmitoylphosphatidylcholine (DPPC) and dihexadecylphosphatidylcholine (DHPC), to measure the interfacial potential associated with dipolar lipid bilayers.[17] Peitzsch et al. calculated the electrostatic potential in the aqueous phase adjacent to model phospholipid bilayers by employing the nonlinear Poisson−Boltzmann equation.[18] Sánchez-Quesada et al. measured ion currents through cyclic peptide nanotubes embedded into two different lipid bilayers, DPPC and glyceryl-monooleate (GMO), and observed a current decrease in the experiment with the DPPC bilayer.[13]

From a theoretical point of view, the cyclic peptide nanotubes provide an important opportunity for insight into the transport of water, ions, and small molecules due to their relatively simple structure. Several theoretical and computational studies have already been done to characterize properties of the cyclic peptide nanotubes other than ion transport. Among these studies, Engels et al. used molecular dynamics (MD) simulations to investigate the dynamics of water inside a cyclic peptide nanotube with hydrophilic side chains.[20] They determined the arrangement of water molecules inside the tubes and computed a water diffusion coefficient that is lower than that of bulk water. Asthagiri and Bashford calculated the solvation energies of ions inside a model cyclic peptide nanotube using several methods,[21] while Tarek et al. performed an MD simulation to examine the configuration of a cyclic peptide nanotube that is embedded into a lipid bilayer membrane.[22]

Theoretical studies of ion transport through ion channels may be done by several methods, but there are significant challenges with using all of them to generate high quality conductivity estimates.[23] MD simulations have been used to elucidate the detailed nature of the transport of water and ions inside ion channels at an atomic level without any parameters other than the assumed force field.[24−26] However, most ion channels contain tens of thousands of atoms,[22] and the time scale (∼10 ns)[1] of transport of even a single ion still makes full atomistic

10.1021/jp055740e CCC: $33.50 © 2006 American Chemical Society
Published on Web 03/15/2006

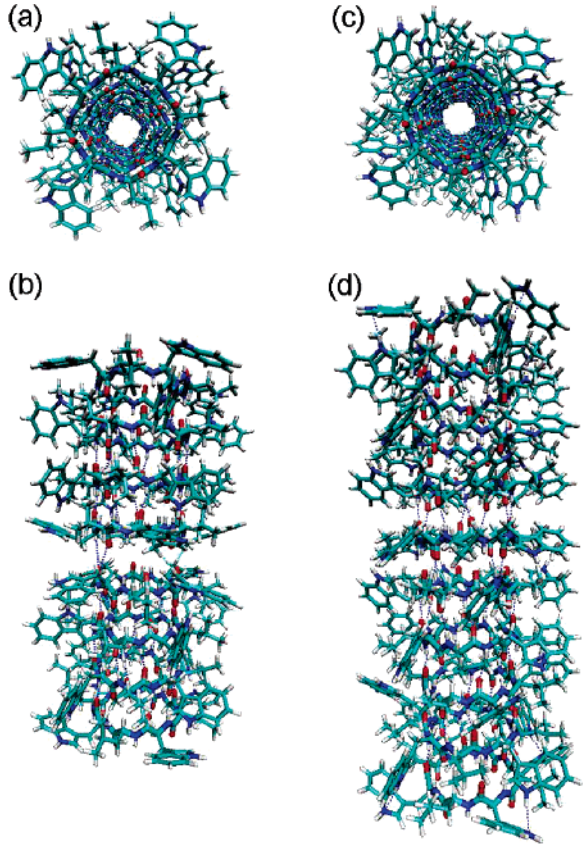

Figure 1. (a), (c) Top view and (b), (d) side view of cyclic peptide nanotubes, 8×cyclo[(-L-Trp-D-Leu-)$_4$] and 10×cyclo[(-L-Trp-D-Leu-)$_4$], respectively. Hydrogen bonds between the cyclic peptide rings are represented with dotted lines.

simulations expensive with current computational resources. An alternative to MD simulation methods is a dielectric continuum method such as the Poisson−Nernst−Planck (PNP) theory.[27,28] Although the ability of this method is limited due to the continuum description of the proteins, water, and ions, the method has proven to describe ion transport reasonably well with appropriate dielectric constants and ion diffusion coefficients. As a result, it has been extensively used in biophysics[27−30] and engineering.[31−33]

In the PNP theory of electrodiffusion, average ion fluxes are determined from the concentration gradient and electrostatic potential. The theory is based on coupling the Poisson and the steady-state diffusion Smoluchowski equations, which are nonlinear differential equations that need to be solved simultaneously and self-consistently.[34] In addition, these coupled equations need to be solved in three dimensions (3D) subject to complex boundary conditions and spatially varying dielectric constants. A variety of numerical approaches to their solution have been pursued. Kurnikova and co-workers proposed a lattice relaxation algorithm for the 3D PNP theory and applied it to the Gramicidin A channel to obtain ion currents.[27] Cárdenas et al. investigated the influence of membrane electrostatics on currents using this same lattice relaxation algorithm.[35] Corry et al. used both PNP theory and Brownian dynamics (BD) in a model channel system to test the validity of the dielectric continuum model.[36]

In this study we use the finite difference method for solving the 3D nonlinear PNP equations to calculate ion currents for cyclic peptide nanotubes formed from eight or ten cyclo[(-L-Trp-D-Leu-)$_4$] subunits (Figure 1).[11] We also examine the electrostatics inside the cyclic peptide tube, and we compare our results with experimental data. We model both GMC and DPPC lipid bilayer membranes to investigate the influence of the membrane dipoles on ion transport. As mentioned above, PNP theory has limitations attributed to the dielectric continuum description. Nevertheless, we believe that the theory provides useful insight into the electrostatics of these nanotubes and the effect of membrane potentials on the ion currents.

This work is organized as follows. In the following section, we briefly review PNP theory and we describe the finite different method for solving the 3D coupled equations. In section 3 the ion currents are calculated for two different types of membranes and the results are compared with the experiment. Our findings are summarized in section 4.

II. Theoretical and Computational Methods

A. PNP Theory. In this section we provide a brief outline of PNP theory. PNP theory is based on coupling the Poisson and steady-state drift-diffusion Smoluchowski equations. The Poisson equation determines the electrostatic potential for a specified distribution of ions. This uses a dielectric continuum description, so the electronic and nuclear polarizations of molecules are described using dielectric constants, and the distributions of ions are expressed as number density functions. The Poisson equation is

$$\nabla[\epsilon(\mathbf{r})\nabla\phi(\mathbf{r})] = -\sum_{\nu} z_\nu e n_\nu(\mathbf{r}) - \rho_f(\mathbf{r}) \tag{1}$$

where $\phi(\mathbf{r})$ is the electrostatic potential due to the ions and to fixed charges in the proteins, $\epsilon(\mathbf{r})$ is the space-dependent dielectric constant, z_ν and $n_\nu(\mathbf{r})$ are the charge and number density of ions of species ν, respectively and $\rho_f(\mathbf{r})$ is the charge density of fixed charges in the proteins.

The Smoluchowski equation describes the diffusion of ions and is given as

$$\frac{\partial n_\nu(\mathbf{r},t)}{\partial t} = -\nabla \mathbf{J}_\nu(\mathbf{r},t) \tag{2}$$

Here the ion flux or the ion current density for an ion species ν, $\mathbf{J}_\nu(\mathbf{r},t)$ under an external field is given by

$$\mathbf{J}_\nu(\mathbf{r},t) = -D_\nu(\mathbf{r})[\nabla n_\nu(\mathbf{r},t) + \beta \nabla w_\nu(\mathbf{r}) n_\nu(\mathbf{r},t)] \tag{3}$$

where $D_\nu(\mathbf{r})$ is the space-dependent diffusion coefficient for ion ν, $w_\nu(\mathbf{r})$ is the potential of mean force (PMF) acting on the species ν, $w_\nu(\mathbf{r}) = z_\nu|e|\phi(\mathbf{r})$, and $\beta = 1/k_BT$. Since the diffusion coefficients inside the ion channels are known to be different from the bulk,[26] we use different values for the diffusion coefficients inside the channel and in bulk. One crucial assumption in PNP theory is that the PMF is governed by the electrostatic potential. This links the Smoluchowski and Poisson equations.

We are interested in the steady-state solution where $\partial n_\nu(\mathbf{r},t)/\partial t = 0$ everywhere, so the flux $\mathbf{J}_\nu(\mathbf{r},t)$ is time-independent and the steady-state solution for Smoluchowski equation satisfies

$$\nabla \mathbf{J}_\nu(\mathbf{r}) = 0 \tag{4}$$

or

$$\nabla D_\nu(\mathbf{r})[\nabla n_\nu(\mathbf{r}) + \beta \nabla w_\nu(\mathbf{r}) n_\nu(\mathbf{r})] = 0 \tag{5}$$

Equation 5 is called the Nernst−Planck (NP) equation. The first term in eq 5 is associated with the diffusion of ions and the second term with their drift motion due to the electrostatic

potential gradient. When there is no ion flux, i.e., $\mathbf{J}_\nu(\mathbf{r}) = 0$, the solution of eq 3 becomes $n_\nu(\mathbf{r}) = n_\nu^0 e^{-\beta w(\mathbf{r})}$ and eq 1 is reduced to the well-known Poisson−Boltzmann (PB) equation:

$$\nabla[\epsilon(\mathbf{r})\nabla\phi(\mathbf{r})] = -\sum_\nu z_\nu e n_\nu^0 e^{-\beta z_\nu |e|\phi(\mathbf{r})} - \rho_f(\mathbf{r}) \qquad (6)$$

where n_ν^0 is the bulk number density of ion ν.

B. Computational Details. The finite difference method has been extensively developed and used in solving the 3D PB equation.[29,37] This method has also been developed to solve the 3D coupled nonlinear equations in PNP theory by several groups.[27,28,36] Here we use the same method as adapted to our particular application.

In this method, eqs 1 and 3 are solved simultaneously and self-consistently until they both reach a set of tolerances. The solution for the electrostatic potential at a grid point (i,j,k), $\phi_{i,j,k}$ is obtained from eq 1 as[28]

$$\phi_{i,j,k} = \epsilon_{i+1,j,k}\phi_{i+1,j,k} + \frac{\epsilon_{k-1,j,k}\phi_{i-1,j,k} + \epsilon_{i,j+1,k}\phi_{i,j+1,k} + \epsilon_{i,j-1,k}\phi_{i,j-1,k}}{\epsilon_{i+1,j,k} + \epsilon_{i-1,j,k} + \epsilon_{i,j+1,k} + \epsilon_{i,j-1,k}} + \frac{\epsilon_{i,j,k+1}\phi_{i,j,k+1} + \epsilon_{i,j,k-1}\phi_{i,j,k-1} + \sum_\nu z_\nu |e|\, h^2 n_{i,j\,k}^\nu + q_{i,j,k}/h}{+\epsilon_{i,j,k+1} + \epsilon_{i,j,k-1}} \qquad (7)$$

where h is the grid length in any direction and the $q_{i,j,k}$ is the charge assigned at the grid point (i,j,k). We assume that the grid length in each direction is the same.

The steady-state solution for the number density at grid point (i,j,k), $n_{i,j,k}^\nu$ can be obtained from eq 3 and eq 4. The final form is then written as[27,28]

$$n_{i,j,k}^\nu = \frac{n_{i+1,j,k}^\nu\{1+\beta z_\nu|e|(\phi_{i+1,j,k}-\phi_{i,j,k})/2\} + n_{i-1,j,k}^\nu\{1+\beta z_\nu|e|(\phi_{i-1,j,k}-\phi_{i,j,k})/2\}}{6 - \beta z_\nu|e|(\phi_{i+1,j,k} - \phi_{i,j,k})/2 - \beta z_\nu|e|(\phi_{i-1,j,k} - \phi_{i,j,k})/2} + \frac{n_{i,j+1,k}^\nu\{1+\beta z_\nu|e|(\phi_{i,j+1,k}-\phi_{i,j,k})/2\} + n_{i,j-1,k}^\nu\{1+\beta z_\nu|e|(\phi_{i,j-1,k}-\phi_{i,j,k})/2\}}{- \beta z_\nu|e|(\phi_{i,j+1,k} - \phi_{i,j,k})/2 - \beta z_\nu|e|(\phi_{i,j-1,k} - \phi_{i,j,k})/2} + \frac{n_{i,j,k+1}^\nu\{1 + \beta z_\nu|e|(\phi_{i,j,k+1}-\phi_{i,j,k})/2\} + n_{i,j,k-1}^\nu\{1+\beta z_\nu|e|(\phi_{i,j,k-1}-\phi_{i,j,k})/2\}}{-\beta z_\nu|e|(\phi_{i,j,k+1} - \phi_{i,j,k})/2 - \beta z_\nu|e|(\phi_{i,j,k-1} - \phi_{i,j,k})/2} \qquad (8)$$

The current density for ion ν at a grid point (i,j,k), $J_{i,j,k}^\nu$, can be calculated using

$$J_{i,j,k}^\nu = -D_\nu \frac{n_{i,j,k}^\nu - n_{i,j,k-1}^\nu}{h} + \frac{\beta z_\nu|e|(n_{i,j,k}^\nu + n_{i,j,k-1}^\nu)(\phi_{i,j,k} - \phi_{i,j,k-1})}{2h} \qquad (9)$$

One of the most important problems in the finite difference method is how to assign charges and dielectric constants at each grid point. This problem occurs because a system based on a continuum description is mapped onto a discrete model system through the finite difference method.

Several methods have been proposed to map the distribution of charges onto the grids.[29,38−40] We use the antialias method proposed by Bruccoleri et al.[40] In this method, the charge density is specified in proportion to the fraction of the cube that is occupied by each atom. The advantage of this method over other methods is that the dependence of the total electrostatic potential energy on grid spacing is reduced and the convergence for the self-energy is improved.

We generate a dielectric constant map with the method proposed by Gilson et al.[29] The first step of this method is to define protein, membrane, and solvent regions as was done by Richards.[41] Next, we define a grid line center as the middle point of the line connecting two neighboring grid points. Then the dielectric constants for the protein, membrane, and solvent are assigned to the grid line centers which are contained in each region.

We use different values for the diffusion coefficients in the channel and in the bulk. These are assigned to each grid point using

$$D_{i,j,k} = D^{\mathrm{chn}} n_{i,j,k}^{\mathrm{chn}}/6 + D^{\mathrm{blk}} n_{i,j,k}^{\mathrm{blk}}/6 \qquad (10)$$

where D^{chn} and D^{blk} are the inside-channel and bulk diffusion coefficients, respectively, and $n_{i,j,k}^{\mathrm{chn}}$ and $n_{i,j,k}^{\mathrm{blk}}$ are the numbers of grid lines (from 0 to 6) attached to a grid point (i,j,k) whose center is assigned to the channel or bulk solvent regions.

C. Construction of Cyclic Peptide Nanotubes, 8×Cyclo-[(-L-Trp-D-Leu-)$_4$] and 10×cyclo[(-L-Trp-D-Leu-)$_4$]. An eight-residue cyclic L-peptide ring with an alternating sequence of L-Trp and D-Leu residues was constructed using the SPARTAN molecular modeling package.[42] Based on single channel conductance experiments[9] and other studies on ion channels,[22] we assumed that, depending on the thickness of lipid bilayers considered in our study, eight (for the GMO lipid bilayer) or 10 (for the DPPC lipid bilayer) cyclic peptide rings are self-assembled in the lipid membrane to form cyclic peptide nanotubes, 8×cyclo[(-L-Trp-D-Leu-)$_4$] or 10×cyclo[(-L-Trp-D-Leu-)$_4$];[11] see Figure 1.

Due to the alternating order of the L-Trp and D-Leu residues, all hydrophobic side chains are oriented outside. We then performed an energy minimization of the cyclic peptide nanotubes with the all-atom CHARMM27 force field[43] using NAMD version 2.5.[44] In the energy-minimized structure of the nanotubes, the average distance between two cyclic peptide rings is about 4.85 Å, and the average radius of a ring from the central axis to C_α atoms on the tube is 4.87 Å. We employed this structure of the cyclic peptide nanotube for all the 3D PNP calculations.

3D PNP calculations require partial charges and van der Waals radii for all atoms to calculate the electrostatic potentials and to define solvent-exclusion regions. We used the CHARMM27 force field for that purpose. The central axis of the cyclic peptide nanotube in our system is assumed to be approximately perpendicular to the membrane surfaces.

III. Results

A. Model Case. To ensure that our PNP code works properly, we first solve a simple model system where the solutions for ion currents and ion concentrations can be obtained analytically.[27,28] As shown in Figure 2, we consider a cylindrical system that is homogeneous in the x and y directions with an external field applied to the top and bottom. The cations and anions inside the cylinder do not interact with each other, but interact only with the applied field. The applied field is assumed to be linear as follows:

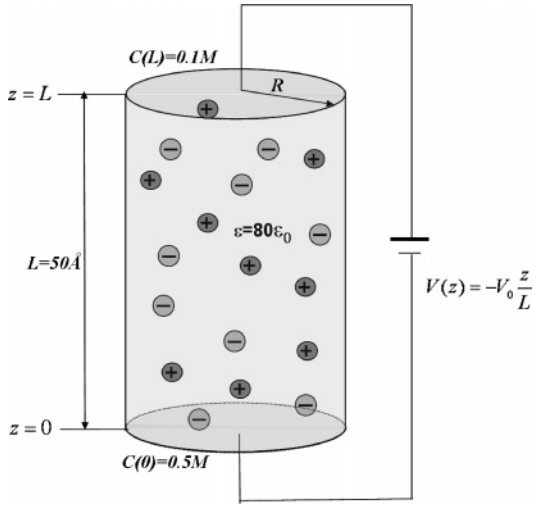

Figure 2. Model system with cylindrical symmetry. System parameters are indicated. The applied voltage is assumed to vary linearly along the length of the cylinder.

$$V(z) = -V_0\frac{z}{L} \tag{11}$$

where V_0 is the voltage difference between the bottom and the top of the cylinder and L is the cylinder length.

Since the system is homogeneous in the x and y directions, we can generate 1D solutions for the steady-state number density to eq 5 as follows:

$$n_\nu(z) = \exp\frac{\beta z_\nu |e| V_0}{L} z \times \left\{ n_\nu(0) + (n_\nu(L)\exp[-\beta z_\nu |e| V_0] - n_\nu(0)) \frac{\exp[-\beta z_\nu |e| V_0 z/L] - 1}{\exp[-\beta z_\nu |e| V_0] - 1} \right\} \tag{12}$$

and for the current density:

$$J_\nu = \frac{D_\nu \beta z_\nu |e| V_0}{L} \cdot \frac{n_\nu(L)\exp[-\beta z_\nu |e| V_0] - n_\nu(0)}{\exp[-\beta z_\nu |e| V_0] - 1} \tag{13}$$

For numerical calculations, the length (L) of the cylinder in the z direction is taken to be 50 Å and the radius (R) of the cylinder is 4 Å. The ion concentrations at the bottom and top are 0.5 and 0.1 M, respectively. The 3D PNP calculations are performed on a 100 × 100 × 100 grid with a grid size of 0.5 Å. Ions are assumed to be monovalent, and a diffusion coefficient of 1.96×10^{-5} cm^2/s is used for both cations and anions. The dielectric constant is 80 ϵ_0 everywhere.

Figure 3a shows current density−voltage curves for the cation calculated with our 3D PNP code and with eq 14. The numerical results are in excellent agreement with the analytical solutions. Due to the different concentrations of ions at the bottom and top of the cylinder, a nonzero ion current at zero voltage is observed. We found negligible variation of the results with the cylinder radius, R. The cation concentrations for several voltages are presented in Figure 3b. Again there is excellent agreement between the numerical and analytical results.

B. Ion Currents in GMO Lipid Bilayer Membranes. In this calculation, the cyclic peptide nanotube is embedded in a GMO lipid bilayer membrane and placed in a KCl solution. GMO lipids are popularly used to construct bilayer membranes.

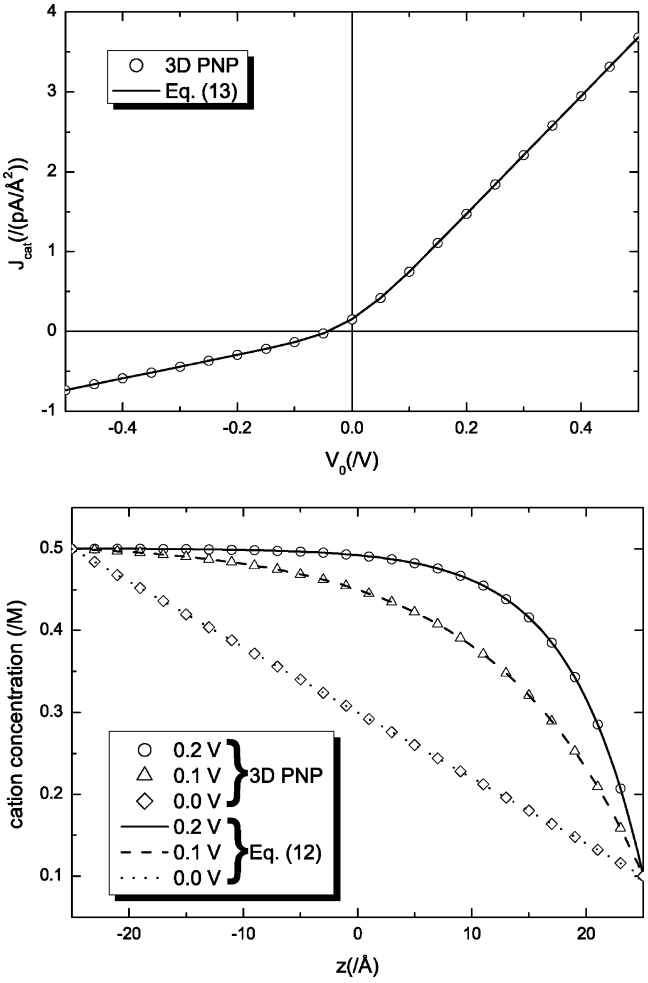

Figure 3. (a) Cationic current density versus voltage for the model system comparing the numerical PNP results and analytical results derived from eq 14. Here the ion concentrations at the bottom and top of the cylinder are 0.5 and 0.1 M, respectively. (b) Concentration profiles for different applied voltages. The same boundary condition as in (a) is used.

Since GMO molecules do not possess any dipoles, we assume that the GMO membrane is a nonpolar dielectric material. We take the thickness of the GMO membrane to be 33 Å. The same value was used by Cárdenas et al. to model this for a different ion channel. Taking the thickness of the GMO lipid bilayer into account, we assume that eight cyclic peptide rings are self-assembled in the GMO bilayer.

The dielectric constant is one of the most important parameters in PNP theory. For protein-like ion channels, low values from 4 ϵ_0 to 20 ϵ_0 have been used to incorporate the restrictions in the orientational and vibrational polarizations of proteins.[27,28,32,45] Since the lipid molecules in the membrane are well packed, low dielectric constants have also been assigned to the bilayer membrane, varying from 2 ϵ_0 to 4 ϵ_0.[27,32,45,46] We speculate that the cyclic peptide nanotube, which has a tubular structure because of hydrogen bonding, has a higher dielectric constant than that of the membrane because the restriction in nuclear polarization is lifted to some degree by the weaker interactions (from hydrogen bonding) between the peptide rings. As a result, the dielectric constants in our calculations are selected to be 4 ϵ_0, 2 ϵ_0, and 80 ϵ_0 for the cyclic peptide nanotube, GMO membrane, and water, respectively.

MD simulations have shown that the motions of ions inside ion channels are slower than in bulk partly due to the strong ion correlations arising from the higher concentration of ions

inside the channel and partly to the electrostatic interaction between ions and partial charges in the channel.[26,47] Following these results, we use different ion diffusion coefficients in the bulk and inside the nanotube. The bulk diffusion coefficients for K^+ and Cl^- are taken to be 2.0×10^{-5} and 2.0×10^{-5} cm^2/s, respectively, and the corresponding coefficients inside the channel are 0.4×10^{-5} and 0.2×10^{-5} cm^2/s. The values we have chosen for the ion diffusion coefficients inside the tube are within the range of the values used by other groups who studied different ion channels.[26−28,32,36,45]

The concept of a Stern layer has been introduced to describe the ion-exclusion volume associated with contact of ions with the protein surfaces.[48] We use a Stern layer parameter of 1.6 Å in this calculation. It should be noted that, while the selection of parameters in this calculation was guided in part to generate a fit to the experimental data (see below), the values we used have "typical" values whose physical significance is easily understood.

The bulk ion concentration at the bottom and top of the tube are fixed at 0.1 M. The concentration of ions on the side walls of the system is considered to be zero. We also tried periodic boundary conditions, but the results did not depend on this boundary condition very much. The calculation is performed on a $140 \times 140 \times 140$ grid with a grid size of 0.5 Å. See Figure 4a. The PNP calculations are done twice for each applied voltage, once for the configuration of the energy-minimized nanotube, and once for the upside-down configuration of the nanotube, to take the simplest configuration average into account.

Figure 5 shows the calculated current−voltage curves. The presence of negative charges due to carbonyl oxygens inside the peptide nanotube allows K^+ to flow through the tube, but prevents Cl^- from crossing. As a result, the K^+ ion currents are significantly larger than the Cl^- currents. In fact, our calculation shows an almost negligible Cl^- current. We estimate the ratio of the K^+ current to the Cl^- current to be 1.7×10^3, which reveals the strong selectivity of the peptide nanotube to cations. Although Ghadiri et al. do not quote a value for this ratio, they did suggest that, because of the high cation selectivity, this type of cyclic peptide nanotube can be used in the design of ligand-gated channels for stochastic sensing.[13] We find that the ion current in the tube has a nearly linear variation with voltage, with a total conductance of 35.9 pS.

The experimental conductance for the cyclic peptide nanotube in the GMO bilayer can be obtained by using the Michaelis−Menten saturation model with the parameters provided in ref 13. The Michaelis−Menten saturation model for conductance, Λ, is given as[1]

$$\Lambda = \frac{\Lambda_{max}}{1 + K_m/[I]} \tag{14}$$

where Λ_{max} is the maximum conductance and $[I]$ is the ion concentration. Given $\Lambda_{max} = 44.2$ pS and $K_m = 50.0 \times 10^{-3}$ M in the GMO bilayer, the experimental conductance at the ion concentration of 0.1 M is 29.5 pS, which is comparable to our calculated value, 35.9 pS.

Figure 6a shows the electrostatic potentials for two choices of the voltages. We observe a large potential drop inside the channel due to the negatively charged carbonyl oxygens on the tube. Before we discuss further, we define two regions inside the peptide nanotube following Engels et al.[20] The regions near the plane of the peptide C_α atoms in a cyclic peptide ring are defined as the α-plane zone and the regions between two

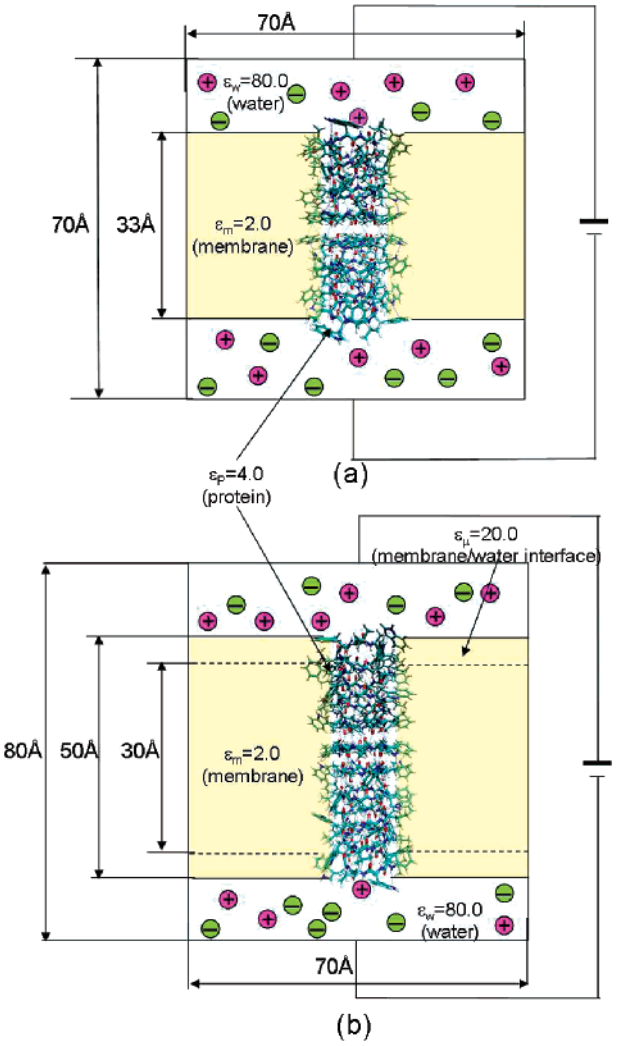

Figure 4. (a) Description of the cyclic peptide nanotube embedded in a GMO lipid bilayer and surrounded by KCl solution. System dimensions and dielectric constants used are indicated. (b) The corresponding description of the nanotube with DPPC lipid bilayer, including contraction of the DPPC bilayer.

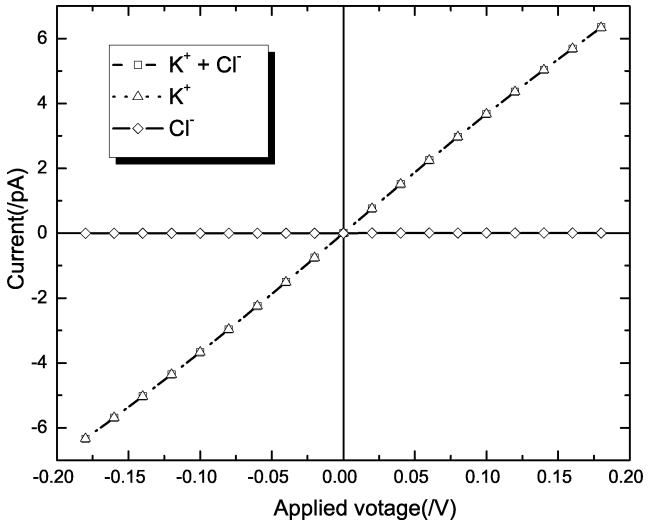

Figure 5. Current−voltage curves for $K^+ + Cl^-$, K^+, and Cl^- in the cyclic peptide nanotube embedded in a GMO bilayer. The bulk ion concentrations at the bottom and top are both 0.1 M.

α-plane zones as the midplane zones. Then we see several wells whose positions correspond to midplane zones in the electro-

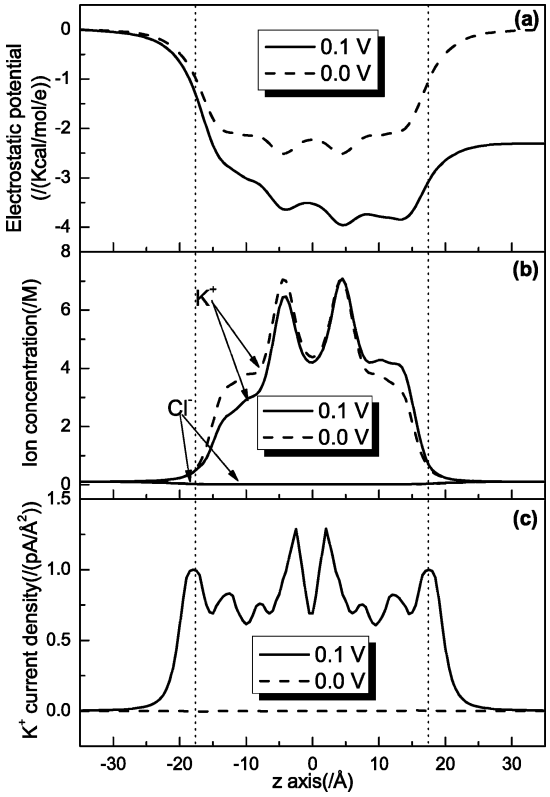

Figure 6. (a) Electrostatic potentials, (b) K^+ and Cl^- concentrations, and (c) K^+ current densities at two different applied voltages for the cyclic peptide nanotube in GMO bilayer. The dotted lines represent the channel entrances located at ± 17.0 Å. The channel entrances are defined by the positions of the first and last C_α planes in the *z* direction. The concentration boundary is the same as in the previous figure.

static potentials. This shows that electrostatically K^+ is more stable in the midplane zones rather than in the α-plane zones. As a result, the concentration of K^+ is higher in the midplane zones in Figure 6b. The ion selectivity is also shown clearly from the concentration profiles. As a result of the attractions between K^+ and the negative charges of the carbonyl oxygens inside the nanotube, the concentration of K^+ is very high inside the tube. At the same time, the concentration of Cl^- is minimal due to the repulsion between negative charges. While the concentration profile is symmetric along the *z* axis at zero voltage, it is not symmetric when a voltage is applied.

The ion current can be cast as

$$I = J(z)A(z) \tag{15}$$

where $J(z)$ is the ion current density or ion flux and $A(z)$ is the cross section through which ions flow. Although current should not depend on position along the *z* axis, $J(z)$ and $A(z)$ do. Since the areas occupied by the α-plane zones are smaller than those by the midplane zones, the current density should be larger in the α-plane zones to keep the current constant. Consequently, Figure 6c shows eight peaks which correspond to the current density in the α-plane zones. This current density profile partially reflects the structure of the cyclic peptide nanotube.

The dependence of the ion currents on the dielectric constant of the cyclic peptide nanotube is examined in Figure 7. An increase of the dielectric constant of the nanotube reduces the cation currents because the higher dielectric constant makes the electrostatic interaction between the cations and the carboxyl oxygens in the nanotube weaker due to stronger screening. Although the anion currents increase as the dielectric constant increases, they still make little contribution to the total currents and they are not shown in Figure 7.

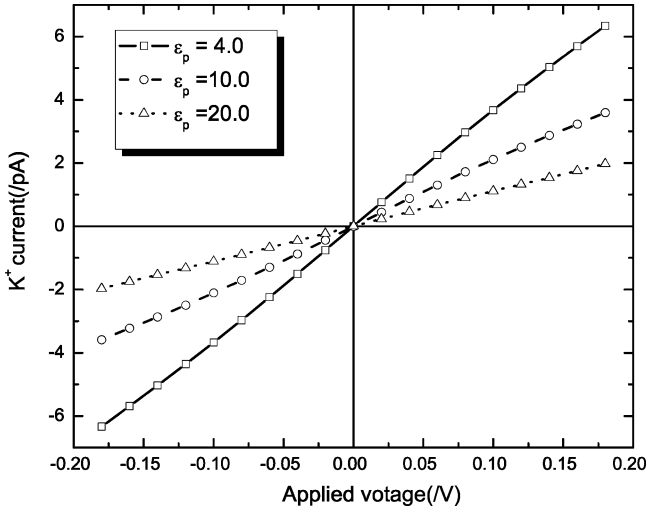

Figure 7. Dependence of cation currents on the dielectric constant of the cyclic peptide nanotube. Only the cation currents are shown since the anion currents are minimal and do not contribute to the total currents. The other parameters are the same.

C. Ion Currents for Nanotubes in DPPC Lipid Bilayer. Ion transport can be influenced by electrostatic potentials that arise from polar lipid molecules in the bilayer surrounding the ion channel. Sánchez-Quesada et al. showed that the ion currents decrease when they used dipalmitoylphosphatidylcholine (DPPC) lipid bilayer membranes which have dipoles in the polar headgroups.[13] These dipoles are created by the surface charges of the lipid molecules in combination with oriented solvent water molecules.[17]

To model the interfacial dipole potential at the membrane/water interface, we use a method proposed by Cádenas et al.[35] In that method, dipoles are inserted at each side of the lipid bilayer membrane. Several studies have shown that the dipole potentials are positive inside the membrane with respect to the membrane/water interface,[15,49] so the positive ends of the dipoles are placed inside the membrane and are separated by 10 Å from the negative ends at the interfaces. See Figure 8.

Flewelling and Hubble proposed an equation based on a simple capacitor model to calculate lipid dipole potentials in membrane/water interfaces.[16] According to their model, the dipole potential difference (in volts) at each interface can be written as

$$\Delta V_d \approx 38\frac{\rho_\mu \mu}{\epsilon_\mu} \tag{16}$$

where ρ_μ is the dipole density at each interface (in $Å^{-2}$), μ is the amount of the dipole moment (in Debye), and ϵ_μ is an effective relative dielectric constant associated with the dipoles at an interface. In our calculation, a dipole density of 0.118 $Å^{-2}$ is used, and a charge of ± 0.015*e* on the ± components of each dipole is chosen to make the dipole moment be 0.72 D. Under the assumption that the dielectric constant of the membrane/water interfaces is between that of membrane and that of water, the effective relative dielectric constant at the interfaces is chosen to be 20. Consequently, eq 17 provides a dipole potential of 161 mV for the parameters given above. This value is acceptable compared with experimentally estimated values of 120−200 mV for phosphatidylcholine.[16,49]

We carry out computations of the ion currents for the cyclic peptide nanotube in a DPPC bilayer membrane model using

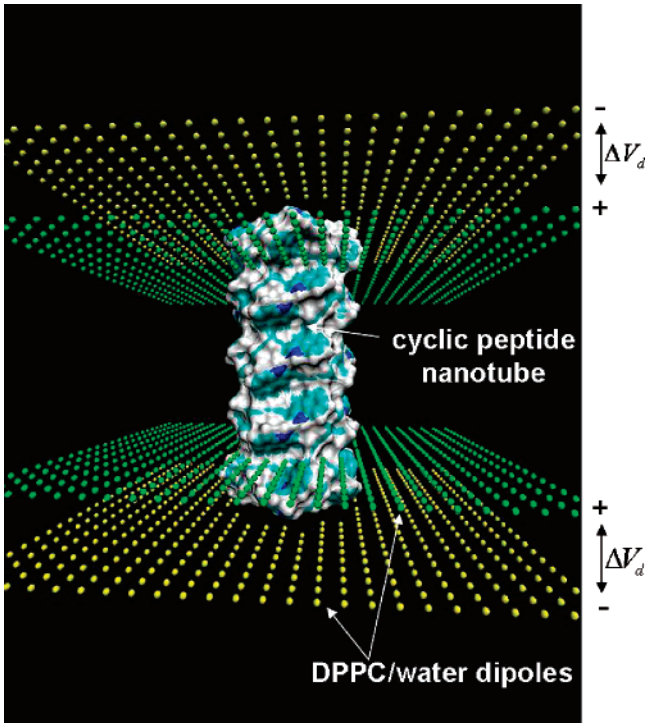

Figure 8. Graphical representation of the cyclic peptide nanotube and DPPC/water dipoles. Negative ends (gray spheres) are placed toward the dipole/water interfaces and positive ends (dark spheres) are placed inside. Contraction of DPPC bilayer is also shown.

the same parameters (dielectric constants and ion diffusion coefficients) as in the previous section. Both cation and anion concentrations in the bulk are 0.1 M. Since the thickness of the DPPC bilayer in our system is estimated to be 50 Å[50] and the distance between two cyclic peptide rings is around 4.85 Å, we assume that 10 cyclic peptide rings are self-assembled to form a peptide nanotube in the DPPC lipid bilayer. To maintain the same distance between the end of the nanotube and the boundary of the system as in the previous GMO model, the system size is increased by 10 Å in the *z* direction. The system dimension and dielectric constants are presented in Figure 4b. The calculation is carried out on a 140 × 140 × 150 grid with a grid size of 0.5 Å. The simplest configuration average as in the previous subsection is considered.

The calculated current−voltage curve in Figure 9 shows good agreement with the experimental data from Sánchez-Quesada et al.[13] The computed conductance of 19.8 pS is also close to the experimental value of 20.1 pS from the Michaelis−Menten saturation model with the parameters, $\Lambda_{max} = 21.5$ pS and $K_m = 7.1 \times 10^{-3}$ M in ref 13.

As seen in the MD and Brownian dynamics (BD) simulations,[51,52] most electrostatic potential drop in Figure 10a occurs across the cyclic peptide nanotube, rather than across the reservoir. Due to the larger number of the cyclic peptide rings assembled in the DPPC bilayer, there are more potential wells than in the GMO lipid bilayer. In Figure 10b, the concentration of K^+ is higher in the midplane zones than in the α-plane zones as in the GMO bilayer. In contrast to the concentration profile in the GMO bilayer, however, the highest peak of the K^+ concentration appears in the middle of the peptide nanotube. Figure 10c shows current densities for K^+ and Cl^- ions. Ten peaks are seen corresponding to the α-plane zones.

To investigate the effect of the lipid dipoles on the ion current, we calculated the ion currents by turning off the charges in the model DPPC lipid/water dipoles. The current−voltage curves

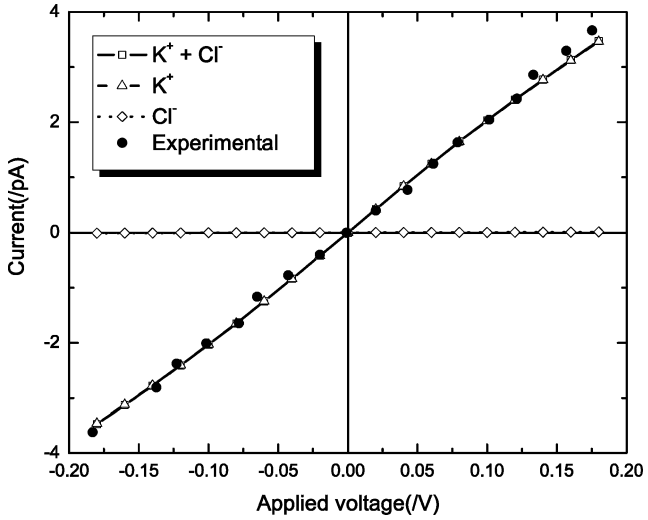

Figure 9. Current−voltage curves for the cyclic peptide nanotube embedded in a DPPC bilayer. Lines are PNP results for K^++Cl^-, K^+, and Cl^- currents, and solid circles are experimental data for $K^+ + Cl^-$ currents from ref 13. The bulk ion concentrations at the bottom and the top are both 0.1 M.

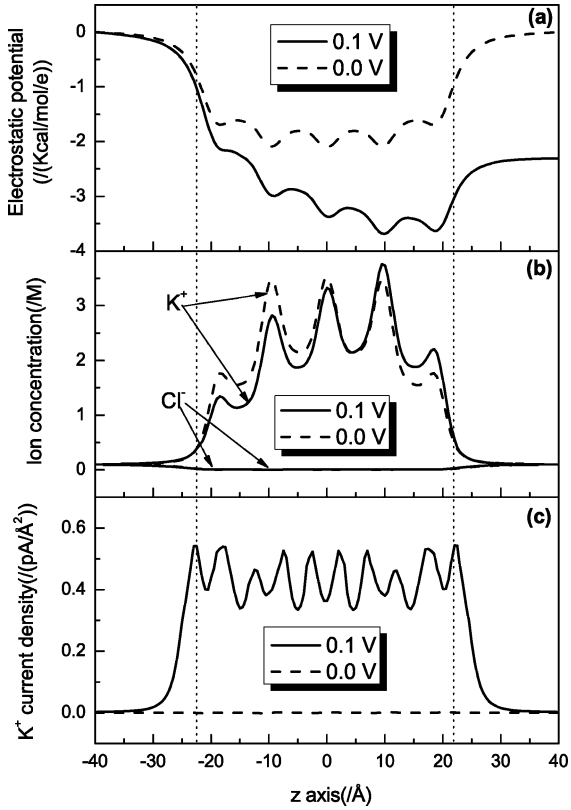

Figure 10. (a) Electrostatic potentials, (b) K^+ and Cl^- concentrations, and (c) K^+ current densities at two different applied voltages in the cyclic peptide nanotube in DPPC bilayer. The concentration boundary is the same as in the previous figure. The dotted lines represent the channel entrances located at ±22.0 Å. The channel entrances are defined by the positions of the first and last C_α planes in the *z* direction.

with and without the lipid/water dipoles are compared in Figure 11a. This shows that the presence of the dipoles at the interface reduces the ion currents. The calculated ion conductance of 19.8 pS with the lipid/water dipoles is to be compared with the conductance of 29.7 pS without the dipoles. The study of Cárdenas and co-workers showed that ion currents also strongly depend on membrane thickness in PNP results for the ion conductance of a Gramicidin A channel embedded in GMO and

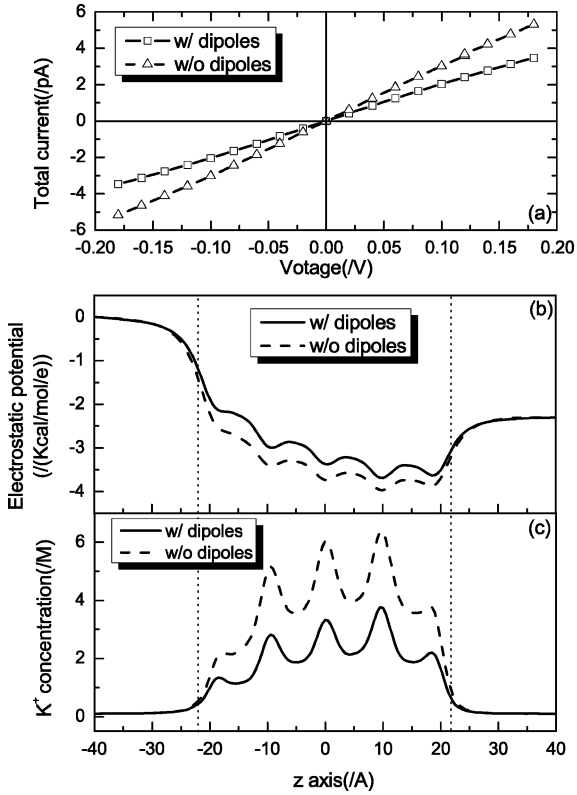

Figure 11. (a) Current−voltage curves with and without lipid/water dipoles in the DPPC bilayer. (b) Electrostatic potentials and (c) K^+ concentrations at the applied voltage of 0.1 V with and without the dipoles in DPPC bilayer. The concentration boundary is the same as in the previous figure.

diphytanoylphosphatidyl choline (DPhPC) lipid membranes.[35] From both results, we speculate that lipid dipoles and membrane thickness are two of the main factors that affect the ion currents in the nanotubes or ion channels.

The electrostatic potentials at the applied voltage of 0.1 V are shown in Figure 11b. This demonstrates that the lipid/water dipoles decrease the electrostatic potential inside the cyclic peptide nanotube. The reduction of the potentials due to lipid dipoles has been reported in previous studies.[35,49] As a result of the reduced electrostatic potential with the dipoles, the K^+ concentration inside the nanotube is lower when there are lipid/water dipoles at the interface (Figure 11c).

We also calculate current−voltage curves for a system where the concentrations are asymmetric, with the bottom concentration being 0.5 M and the top 0.1 M. We can see in Figure 12 that there is still a current at zero voltage due to the concentration gradient. Compared with the conductance of 22.4 pS obtained from the linear fit of the experimental data in Figure 12,[13] our calculated value of 30.8 pS shows that the PNP results overestimate the experimental data.

The drawbacks of PB and PNP theories based on dielectric continuum models have been addressed in the literature,[28,30,36,53,54] and these problems also play a role in assessing the significance of the results we have presented. First of all, the ions have finite sizes in solutions that are larger than in the gas phase due to hydrodynamic interactions with solvent molecules, but dielectric continuum models do not take size into account. Consequently, in the dielectric continuum description, there is excess ion density in the cyclic peptide nanotube, and this can produce ion currents that are too large. Second, collisions and correlations between ions in a confined region such as the ion channel are very strong, and this reduces the ion currents by preventing the

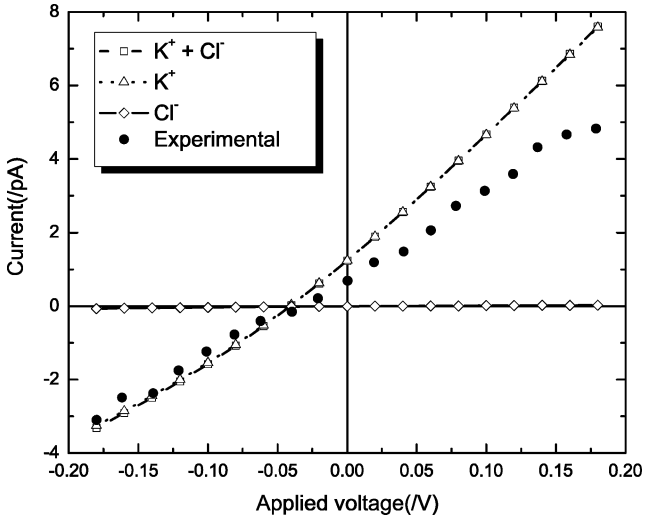

Figure 12. Current−voltage curves of cations, anions, and total in the cyclic peptide nanotube embedded in a DPPC bilayer. Lines are PNP results for $K^+ + Cl^-$, K^+, and Cl^-, and solid circles are experimental data for $K^+ + Cl^-$ from ref 13. The bulk ion concentrations at the bottom and the top are 0.5 and 0.1 M, respectively.

ions from moving freely. However, the dielectric continuum model ignores collisions and correlations between ions and overestimates currents. Finally, when an ion approaches a membrane, it produces an image charge in the membrane. Since the dielectric constant of the membrane is smaller than that of the solvent, this image charge has the same charge as the approaching ion. This leads to a repulsive potential between the approaching ion and the image charge impedes ion flow. This so-called dielectric barrier effect is not included in the original PNP theory.[45,55]

Although the finite size effect is partially included by introducing a Stern layer parameter, that effect is not completely described by this model. In addition, MD simulations have shown that the ion diffusion coefficient decreases as the ion concentration increases due to ion correlation effects.[23,47] Among our input parameters, the inside-channel ion diffusion coefficients and the Stern layer parameter have been optimized to fit the experimental data for a bulk ion concentration of 0.1 M. As a result, we believe that for the inside-channel cation diffusion coefficient, value lower than than 0.4×10^{-5} cm^2/s should be used in our calculation to give a better result when the concentration at the bottom is 0.5 M. The dependence of the ion current on the inside-channel diffusion coefficient is given in Figure 13. Since the contribution of the Cl^- to the current is very small, only the cation diffusion coefficient inside the channel varies. We estimate that a cation diffusion coefficient between 2.5×10^{-5} and 3.0×10^{-5} cm^2/s inside the channel produces the best fit to the experimental data.

Figure 14a shows the electrostatic potentials for the same problem as was considered in Figure 12. The potential for zero applied voltage is not symmetric due to the concentration difference. The gradient of the potential at zero applied voltage gives rise to the small current seen in Figure 12. In Figure 14b the concentration of K^+ at zero applied voltage is asymmetric inside the nanotube due to the different ion concentrations at the bottom and top. The concentrations of Cl^- ions are still minimal inside the tube at either voltage, which shows selectivity to K^+ cations even at high concentrations.

Although a concentration difference exists in the channel, the current densities of K^+ are symmetric since the current density depends on the geometry of the channel rather than the

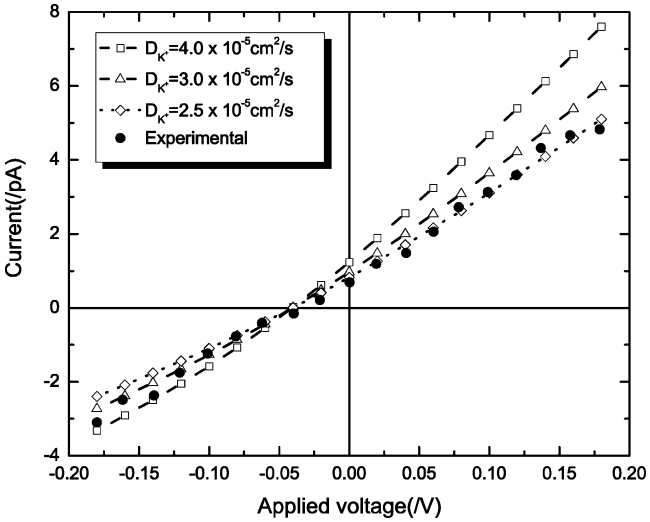

Figure 13. Dependence of ion current on the inside-channel diffusion coefficient. The bulk diffusion coefficient for both cation and anion is 2.0×10^{-5} cm^2/s and the anion diffusion coefficient inside the channel is fixed at 0.2×10^{-5} cm^2/s. Only the cation diffusion coefficient inside the channel varies. The concentration boundary is the same as in the previous figure.

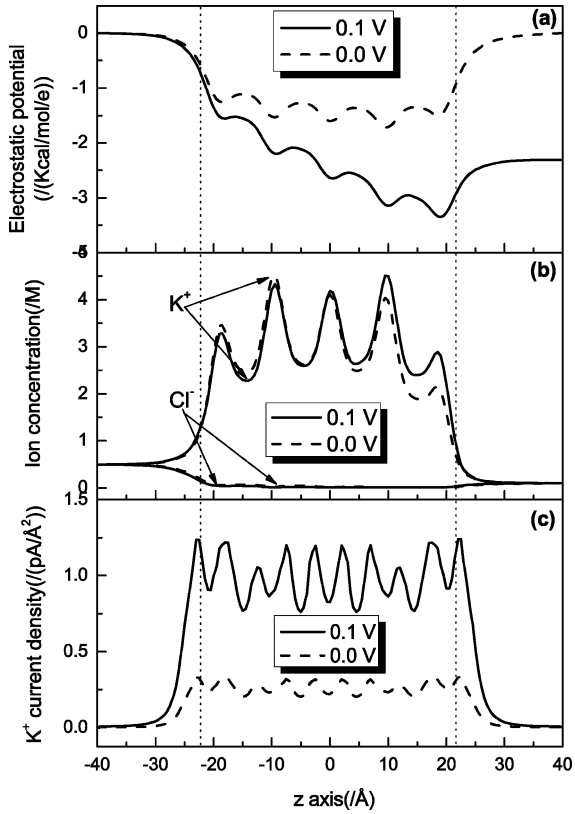

Figure 14. (a) Electrostatic potentials, (b) K^+ and Cl^- concentrations, and (c) K^+ current densities at two different applied voltages for a cyclic peptide nanotube in a DPPC bilayer. The concentration boundary is the same as in the previous figure.

concentration difference. The current densities in Figure 14c bear close resemblance to those in Figure 10c.

IV. Conclusions

In this paper we carried out ion current calculations on a synthetic cyclic peptide nanotube using a finite difference method to solve 3D PNP equations numerically. In our 3D PNP code, the antialias method was implemented to reduce the dependence of the electrostatic energy on grid spacing and to improve the self-energy convergence in the distribution of charges onto grid points.

PNP theory is based on a dielectric continuum model and depends on input parameters such as the dielectric constants of water, protein, and membranes and the diffusion constants of the ions. Although PNP theory has some limitations attributed to uncertainties in these parameters, it has provided some insights into the transport properties of the cyclic peptide nanotubes.

Above all, the current−voltage curves are almost linear for the GMO and the DPPC lipid bilayers when the ion concentrations on either side of the membrane are the same. Comparisons of the calculated current−voltage curves with experimental data showed good agreement in this situation. These comparisons ensure that the selected input parameters in our calculations are reasonable. However, the PNP calculations for the case where there is a concentration difference between the two sides of the membrane overestimate the ion currents. We believe that this overestimation is due to the continuum description that PNP theory relies on.

Our calculation provides insight into the dependence of the ion current on the dielectric constant of the cyclic peptide nanotube. The increase of the dielectric constant of the cyclic peptide nanotube leads to the weaker electrostatic attraction between the cations and the carboxyl oxygens in the nanotube due to stronger screening, and as a result, the ion current decreases.

The concentration profiles clearly show the selectivity of the cyclic peptide nanotubes to cation transport. This selectivity is driven by interactions between the ions and the negatively charged carbonyl oxygens inside the nanotube. The selectivity suggests that the cyclic peptide nanotube can be developed for ion sensing.

The current density calculations show that the current density partially reflects the internal structure of the cyclic peptide nanotube due to the dependence of the current density on the cross section through which ions flow. Indeed we see that the interplay between tube cross sectional area and electrostatic interactions plays a crucial role in determining selectivity.[56] In this sense, the current density calculation can be used to identify the locations of the key regions that limit ion transport.

Our conductance calculations with and without the lipid/water dipoles in the DPPC bilayer show that the ion current in the presence of the dipoles is reduced due to the interaction between the cations and the dipoles. The dependence of the ion currents on the lipid/water dipoles suggests that different types of lipid bilayers with or without dipoles can be employed to control the amount of the ion currents in the nanotube.

There are several issues regarding the underlying assumptions of PNP theory that merit further investigation. As mentioned above, PNP theory does not consider ion size and the correlations between ions and generally overestimates ion concentrations and the currents inside the ion channels. The theory also fails to describe the dielectric barrier effect.

The relative simplicity of the cyclic peptide nanotube suggests that a more sophisticated treatment of ion transport may be possible. MD simulations can be performed to provide better parameters for PNP theory including dielectric constants and ion diffusion coefficients inside the ion channel. Current−voltage calculations at the level of Monte Carlo simulations or Brownian dynamics can be another alternative to account for ion size and correlation effects on ion currents. An approach

based on grand canonical MC simulations is currently under development.

Acknowledgment. This work was supported by the Network for Computational Nanotechnology through a grant from the National Science Foundation. We thank Prof. Reza Ghadiri for helpful suggestions.

References and Notes

(1) Hille, B. *Ionic channels of excitable membranes*; Sinauer Associates Inc.: Massachusettes, 1991.
(2) MacKinnon, R. *Angew. Chem., Int. Ed.* **2004**, *43*, 4265.
(3) Voet, D.; Voet, J. G. *Biochemistry*, 3rd ed.; John Wiley & Sons: New York, 2004; Vol. 1.
(4) Cornell, B. A.; Braach-Maksvytis, V. L. B.; King, L. G.; Osman, P. D. J.; Raguse, B.; Wieczorek, L.; Pace, R. J. *Nature* **1997**, *387*, 580.
(5) Apell, H.-J.; Bamberg, E.; Alpes, H.; Läuger, P. *Membr. Biol.* **1977**, *31*, 171.
(6) Hartgerink, J. D.; Clark, T. D.; Ghadiri, M. R. *Chem. Eur. J.* **1998**, *4*, 1367.
(7) Bayley, H. *Curr. Opin. Biotechnol.* **1999**, *10*, 94.
(8) Ghadiri, M. R.; Granja, J. R.; Milligan, R. A.; McRee, D. E.; Khazanovich, N. *Nature* **1993**, *366*, 324.
(9) Ghadiri, M. R.; Granja, J. R.; Buehler, L. K. *Nature* **1994**, *369*, 301.
(10) Ghadiri, M. R.; Kobayashi, K.; Granja, J. R.; Chadha, R. K.; McRee, D. E. *Angew. Chem. Int. Ed. Engl.* **1995**, *34*, 93.
(11) Motesharei, K.; Ghadiri, M. R. *J. Am. Chem. Soc.* **1997**, *119*, 11306.
(12) Kim, H. S.; Hartgerink, J. D.; Ghadiri, M. R. *J. Am. Chem. Soc.* **1998**, *120*, 4417.
(13) Śanchez-Quesada, J.; Isler, M. P.; Ghadiri, M. R. *J. Am. Chem. Soc.* **2002**, *124*, 10004.
(14) McLaughlin, S. G. A.; Szabo, G.; Eisenman, G.; Ciani, S. M. *Proc. Natl. Acad. Sci. U.S.A.* **1970**, *67*, 1268.
(15) Haydon, D. A.; Myers, V. B. *Biochim. Biophys. Acta* **1973**, *307*, 429.
(16) Flewelling, R. F.; Hubbell, W. L. *Biophys. J.* **1986**, *86*, 541.
(17) Gawrisch, K.; Ruston, D.; Zimmerberg, J.; Parsegian, V. A.; Rand, R. P.; Fuller, N. *Biophys. J.* **1992**, *61*, 1213.
(18) Peitzsch, R. M.; Eisenberg, M.; Sharp, K. A.; McLaughlin, S. *Biophys. J.* **1995**, *68*, 729.
(19) Rostovtseva, T. K.; Aguilella, V. M.; Vodyanoy, I.; Bezrukov, S. M.; Parsegian, V. A. *Biophys. J.* **1998**, *75*, 1783.
(20) Engels, M.; Bashford, D.; Ghadiri, M. R. *J. Am. Chem. Soc.* **1995**, *117*, 9151.
(21) Asthagiri, D.; Bashford, D. *Biophys. J.* **2002**, *82*, 1176.
(22) Tarek, M.; Maigret, B.; Chipot, C. *Biophys. J.* **2003**, *85*, 2287.
(23) Roux, B.; Allen, T.; Berneche, S.; Im, W. *Quart. Rev. Biophys.* **2004**, *37*, 15.
(24) Smith, G. R.; Sansom, S. P. *Biophys. J.* **1998**, *75*, 2767.
(25) Allen, T. W.; Kuyucak, S.; Chung, S.-H. *Biophys. J.* **1999**, *77*, 2502.
(26) Allen, T. W.; Andersen, O. S.; Roux, B. *Proc. Natl. Acad. Sci. U.S.A.* **2004**, *101*, 117.
(27) Kurnikova, M. G.; Coalson, R. D.; Graf, P.; Nitzan, A. *Biophys. J.* **1999**, *76*, 642.
(28) Corry, B.; Kuyucak, S.; Chung, S. H. *Biophys. J.* **2000**, *78*, 2364.
(29) Gilson, M. K.; Sharp, K. A.; Honig, B. H. *J. Comput. Chem.* **1987**, *9*, 327.
(30) Moy, G.; Corry, B.; Kuyucak, S.; Chung, S. H. *Biophys. J.* **2000**, *78*, 2349.
(31) Selberherr, S.; *Analysis and simulation of semiconductor devices*; Springer-Verlag: New York, 1984.
(32) van der Straaten, T. A.; Tang, J.; Eisenberg, R. S.; Ravaioli, U.; Aluru, N. R. *J. Comput. Elec.* **2002**, *1*, 335.
(33) van der Straaten, T. A.; Tang, J.; Ravaioli, U.; Eisenberg, R. S.; Aluru, N. R. *J. Comput. Elec.* **2003**, *2*, 29.
(34) Newman, J. S. *Electrochemical systems*; Prentice Hall Inc.: Englewood Cliffs, New Jersey, 1991.
(35) Cárdenas, A. E.; Coalson, R. D.; Kurnikova, M. G. *Biophys. J.* **2000**, *79*, 80.
(36) Im, W.; Roux, B. *J. Mol. Biol.* **2002**, *322*, 851.
(37) Luty, B. A.; Davis, M. E.; McCammon, J. A. *J. Comput. Chem.* **1992**, *13*, 1114.
(38) Rogers, N. K.; Sternberg, M. J. *J. Mol. Biol.* **1984**, *174*, 527.
(39) Bruccoleri, R. E. *J. Comput. Chem.* **1993**, *14*, 1417.
(40) Bruccoleri, R. E.; Novotny, J.; Davis, M. E. *Annu. Rev. Phys. Chem.* **2000**, *51*, 129.
(41) Richards, F. M. *Annu. Rev. Biophys. Bioeng.* **1977**, *6*, 151.
(42) *Spartan '04*; Wavefunction Inc., 18401 Von Karman Ave., Suite 370 Irvine, California, 2004.
(43) MacKerell, J. A. D.; Bashford, D.; Bellott, M.; Dunbrack, J. R. L.; Evanseck, J.; Field, M. J.; Fischer, S.; Gao, J.; Guo, H.; Ha, S.; Joseph-McCarthy, D.; Kuchnir, L.; Kuczera, K.; Lau, F. T.; Mattos, C.; Michnick, S.; Ngo, T.; Nguyen, D. T.; Prodhom, B.; Reiher, W. E., III; Roux, B.; Schlenkrich, M.; Smith, J. C.; Stote, R.; Straub, J.; Watanabe, M.; Wiórkiewicz-Kuczera, J.; Yin, D.; Karplus, M. *J. Phys. Chem. B* **1998**, *102*, 3586.
(44) Kale, L.; Skeel, R.; Bhandarkar, M.; Brunner, R.; Gursoy, A.; Krawetz, N.; Phillips, J.; Shinozaki, A.; Varadarajan, K.; Schulten, K. *J. Comput. Chem.* **1999**, *151*, 283.
(45) Mamonov, A. B.; Coalson, R. D.; Nitzan, A.; Kurnikova, M. *Biophys. J.* **2003**, *84*, 3646.
(46) Im, W.; Roux, B. *J. Chem. Phys.* **2001**, *115*, 4850.
(47) Chowdhuri, S.; Chandra, A. *J. Chem. Phys.* **2001**, *115*, 3732.
(48) Bard, A. J.; Faulkner, L. R. *Electrochemical methods*; John Wiley & Sons: New York, 1980.
(49) Jordan, P. C. *Membr. Biol. J.* **1984**, *78*, 91.
(50) Nagle, J. F.; Tristram-Nagle, S. *Biochim. Biophys. Acta* **2000**, *1469*, 159.
(51) Crozier, P. S.; Rowley, R. L.; Holladay, N. B.; Henderson, D.; Busath, D. D. *Phys. Rev. Lett.* **2001**, *86*, 2467.
(52) Corry, B.; Hoyles, M.; Allen, T. W.; Walker, M.; Kuyucak, S.; Chung, S.-H. *Biophys. J.* **2002**, *82*, 1975.
(53) Graf, P.; Nitzan, A.; Kurnikova, M. G.; Coalson, R. D. *J. Phys. Chem. B* **2000**, *104*, 12324.
(54) Graf, P.; Kurnikova, M. G.; Coalson, R. D.; Nitzan, A. *J. Phys. Chem. B* **2004**, *108*, 2006.
(55) Corry, B.; Kuyucak, S.; Chung, S. H. *Biophys. J.* **2003**, *84*, 3594.
(56) Doyle, D. A.; Cabral, J. M.; Pfuetzner, R. A.; Kuo, A.; Gulbis, J. M.; Cohen, S. L.; Chait, B. T.; MacKinnon, R. *Science* **1998**, *280*, 69.